



Communication

Surface Adsorption of the Alpha-Emitter Astatine-211 to Gold Nanoparticles Is Stable In Vivo and Potentially Useful in Radionuclide Therapy

Emanuel Sporer ¹, Christian B. M. Poulie ², Sture Lindegren ³, Emma Aneheim ³, Holger Jensen ⁴, Tom Bäck ³, Paul J. Kempen ^{1,5}, Andreas Kjaer ^{4,6}, Matthias M. Herth ^{2,4,*} and Andreas I. Jensen ^{1,*}

- ¹ Center for Nanomedicine and Theranostics, DTU Health Technology, Technical University of Denmark (DTU), Ørstedes Plads 345C, 2800 Lyngby, Denmark; emspo@dtu.dk (E.S.); pkem@dtu.dk (P.J.K.)
 - ² Department of Drug Design and Pharmacology, Faculty of Health and Medical Sciences, University of Copenhagen, Universitetsparken 2, 2100 Copenhagen, Denmark; christian.poulie@sund.ku.dk
 - ³ Departments of Radiation Physics, Institute of Clinical Sciences, Sahlgrenska Academy, University of Gothenburg, Gula Stråket 2b, 41345 Gothenburg, Sweden; sture.lindegren@radfys.gu.se (S.L.); emma.aneheim@radfys.gu.se (E.A.); tom.back@radfys.gu.se (T.B.)
 - ⁴ Department of Clinical Physiology, Nuclear Medicine & PET, Rigshospitalet, Blegdamsvej 9, 2100 Copenhagen, Denmark; holger.jensen@rh.regionh.dk (H.J.); akjaer@sund.ku.dk (A.K.)
 - ⁵ National Centre for Nano Fabrication and Characterization, Technical University of Denmark (DTU), Ørstedes Plads—Building 347, 2800 Lyngby, Denmark
 - ⁶ Cluster for Molecular Imaging, Department of Biomedical Sciences, University of Copenhagen, Blegdamsvej 3, 2100 Copenhagen, Denmark
- * Correspondence: matthias.herth@sund.ku.dk (M.M.H.); atije@dtu.dk (A.I.J.)



Citation: Sporer, E.; Poulie, C.B.M.; Lindegren, S.; Aneheim, E.; Jensen, H.; Bäck, T.; Kempen, P.J.; Kjaer, A.; Herth, M.M.; Jensen, A.I. Surface Adsorption of the Alpha-Emitter Astatine-211 to Gold Nanoparticles Is Stable In Vivo and Potentially Useful in Radionuclide Therapy. *J. Nanotheranostics* **2021**, *2*, 196–207. <https://doi.org/10.3390/jnt2040012>

Academic Editor: Mukesh K. Pandey

Received: 3 August 2021

Accepted: 24 September 2021

Published: 1 October 2021

Publisher's Note: MDPI stays neutral with regard to jurisdictional claims in published maps and institutional affiliations.



Copyright: © 2021 by the authors. Licensee MDPI, Basel, Switzerland. This article is an open access article distributed under the terms and conditions of the Creative Commons Attribution (CC BY) license (<https://creativecommons.org/licenses/by/4.0/>).

Abstract: Targeted α -therapy (TAT) can eradicate tumor metastases while limiting overall toxicity. One of the most promising α -particle emitters is astatine-211 (^{211}At). However, ^{211}At -carbon bonds are notoriously unstable in vivo and no chelators are available. This hampers its adoption in TAT. In this study, the stability of ^{211}At on the surface of gold nanoparticles (AuNPs) was investigated. The employed AuNPs had sizes in the 25–50 nm range. Radiolabeling by non-specific surface-adsorption in >99% radiochemical yield was achieved by mixing ^{211}At and AuNPs both before and after polyethylene glycol (PEG) coating. The resulting ^{211}At -AuNPs were first challenged by harsh oxidation with sodium hypochlorite, removing roughly 50% of the attached ^{211}At . Second, incubation in mouse serum followed by a customized stability test, showed a stability of >95% after 4 h in serum. This high stability was further confirmed in an in vivo study, with comparison to a control group of free ^{211}At . The AuNP-associated ^{211}At showed low uptake in stomach and thyroid, which are hallmark organs of uptake of free ^{211}At , combined with long circulation and high liver and spleen uptake, consistent with nanoparticle biodistribution. These results support that gold surface-adsorbed ^{211}At has high biological stability and is a potentially useful delivery system in TAT.

Keywords: astatine-211; targeted alpha-therapy; gold nanoparticles; radionuclides

1. Introduction

In recent years, targeted α -therapy (TAT) in the treatment of cancer has received increasing interest [1,2]. Clinical α -therapy was spearheaded by the FDA approval of $^{223}\text{RaCl}_2$ (Xofigo[®]) for bone metastases in prostate cancer [3], and ^{225}Ac -PSMA-617 recently showed promise in early clinical trials for metastatic prostate cancer [4,5]. α -particles have substantially higher linear energy transfer (LET) than the widely employed β -particles. This increases their efficacy through a higher propensity for causing double stranded DNA breaks, which often result in cell-cycle arrest followed by mitotic cell death, apoptosis or necrosis [6–8]. Further, the short range in tissue of α -particles (50–100 μm) makes them particularly well-suited for treating micrometastases, a major cause of cancer mortality, as well as reducing unwanted cytotoxicity to healthy surrounding cells [8].

Only a few of the available α -emitters have suitable decay properties for use in TAT, the most prominent examples being actinium-225 (^{225}Ac , $t_{1/2} = 9.9$ d), radium-223 (^{223}Ra , $t_{1/2} = 11.4$ d), thorium-227 (^{227}Th , $t_{1/2} = 18.7$ d), bismuth-212 (^{212}Bi , $t_{1/2} = 60.5$ min), bismuth-213 (^{213}Bi , $t_{1/2} = 46$ min), and astatine-211 (^{211}At , $t_{1/2} = 7.2$ h). Of these, ^{211}At is regarded as having the most optimal decay properties [9]. ^{211}At decays by two branches, either by α -particle emission to bismuth-207 (^{207}Bi) or by electron capture to polonium-211 (^{211}Po) (Figure 1). ^{211}Po in turn decays by α -particle emission to lead-207 (^{207}Pb) with a very short half-life (0.52 s). This means that each decay results in the emission of exactly one α -particle. In contrast, the decays of ^{225}Ac , ^{227}Th and ^{223}Ra result in several α -active daughters, which is believed to have an unfavorable influence on side effects. Further, the half-life of ^{211}At of 7.2 h is well suited for TAT with popular small-molecule and peptide-based vectors, and its production on cyclotrons can be scaled up for global supply [9].

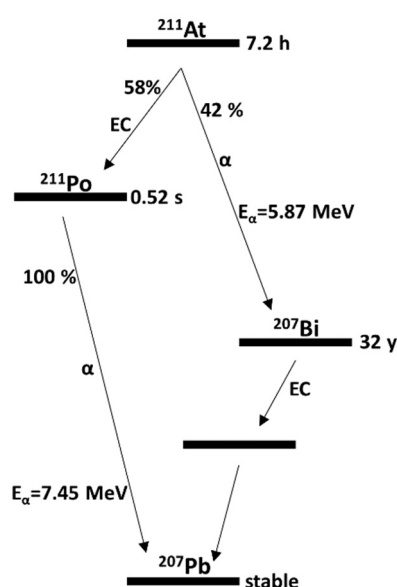


Figure 1. Decay scheme of ^{211}At (modified from Lindegren 2020) [9].

A primary reason for the limited use of ^{211}At has been its challenging radiochemistry. As the heaviest halogen, ^{211}At shares several properties with iodine. However, the halogen-aryl bond is significantly weaker for astatine than it is for iodine [10]. The standard method for forming the astatine-aryl bond is through electrophilic aromatic substitution on trialkyl(aryl)stannane precursors [11–13]. This strategy is useful, but deastatination is commonly observed in vivo [14], likely through intracellular oxidation, followed by homolytic bond cleavage [15].

As an alternative to the astatine-aryl bond, metallic nanoparticles have therefore been investigated for ^{211}At delivery, using non-covalent approaches. Non-specific surface adsorption of ^{211}At was first shown with silver nanoparticles, which were proposed as a carrier system [16,17]. However, gold nanoparticles (AuNPs) are easier to functionalize and have high biocompatibility [18]. AuNPs were recently investigated in pioneering work by Bilewicz and co-workers, using radio-TLC to indicate appreciable serum stability of ^{211}At that was surface-adsorbed onto peptide-modified AuNPs [19,20]. In addition, a high computationally determined stability of ^{211}At on gold clusters was reported [21].

To further investigate the potential use of the surface-adsorption radiolabeling technique in radionuclide therapy, we prepared AuNPs coated with thiolized polyethylene glycol (HS-PEG₅₀₀₀). ^{211}At was surface-adsorbed onto these AuNPs and the stability of this radiolabel was investigated (Figure 2). In this study, we report excellent stability in serum of these ^{211}At -AuNPs, demonstrated through a newly designed method. Further, we report high stability in vivo, demonstrated by quantifying the biodistribution of the

AuNP-borne ^{211}At in mice. Our results demonstrate that surface adsorption of ^{211}At on AuNPs is very stable in biological environments, including in vivo, and that AuNPs are a viable delivery vector in TAT with ^{211}At .

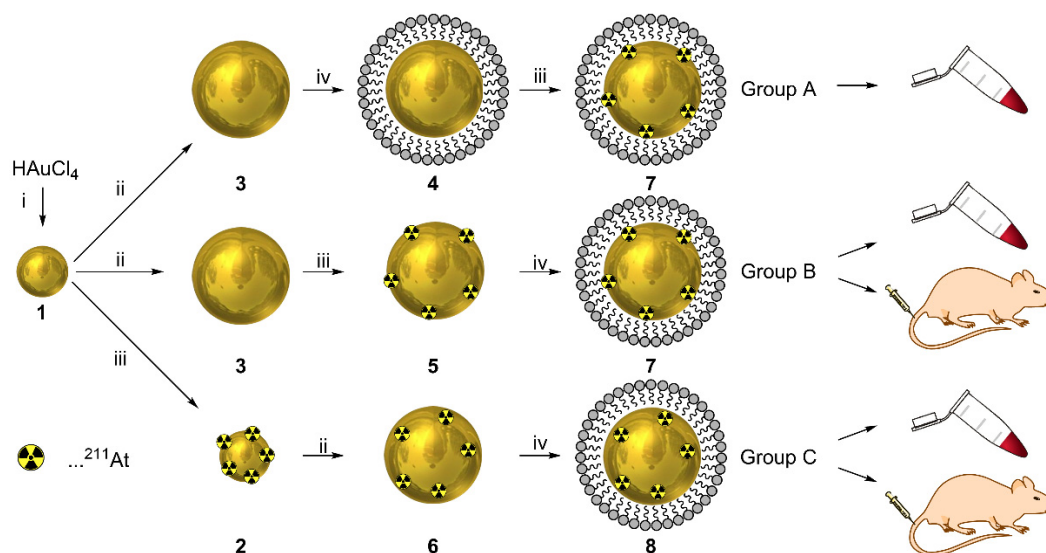


Figure 2. Study design and ^{211}At -AuNPs preparation. The stability of Group A was investigated in serum only; Group B and Group C were investigated both in serum and in mice. Reaction conditions: (i) sodium citrate at 80 °C for 1 h, (ii) slow addition of HAuCl_4 at 80 °C over 6 min and additional reaction time for 1 h, (iii) addition of ^{211}At in chloroform at room temperature and stirred for 20 min, (iv) addition of HS-PEG₅₀₀₀ in water at room temperature and stirred for 25 min. (1) 1st generation citrate-stabilized AuNPs, (2) 1st generation citrate-stabilized [^{211}At]AuNPs, (3) 2nd generation citrate-stabilized AuNPs, (4) 2nd generation HS-PEG₅₀₀₀-coated AuNPs, (5) 2nd generation citrate-stabilized [^{211}At]AuNPs, (6) 2nd generation citrate-stabilized embedded [^{211}At]AuNPs, (7) 2nd generation HS-PEG₅₀₀₀-coated [^{211}At]AuNPs, (8) 2nd generation HS-PEG₅₀₀₀-coated embedded [^{211}At]AuNPs.

2. Materials and Methods

2.1. Materials

Milli-Q (MQ) water (18.2 M Ω × cm) was used for all preparation steps. All glassware and magnetic stirring bars were cleaned with freshly prepared aqua regia (HCl: HNO₃, 3:1, v/v) and rinsed five times with MQ water before use. All chemicals were purchased from Sigma-Aldrich if not stated otherwise. AuNP sizes and Zeta potentials were measured by dynamic light scattering (DLS) on a ZetaPALS (Brookhaven). Metal content of samples was quantified with an ICAP 7000 ICP-OES (Thermo Scientific). ^{211}At activity was measured on a dose calibrator (VEENSTRA instruments), unless otherwise noted. An isotonic HEPES-saline buffer containing 4-(2-hydroxyethyl)-1-piperazineethanesulfonic acid (HEPES, 10 mM) and NaCl (150 mM) was prepared by mixing equal molar amounts of sodium HEPES salt and free acid HEPES, for a final pH of 7.4–7.5 and osmolality of about 290 mOsm/kg. An overview of the synthetic approach can be seen in Figure 2.

2.2. Production of ^{211}At

Stable bismuth deposited on aluminium backing was irradiated with 29 MeV α -particles to produce ^{211}At in a Scanditronix MC32 cyclotron at the positron emission tomography (PET) and Cyclotron Unit at Copenhagen University Hospital, Denmark. At the Department of Nuclear Medicine, Sahlgrenska University Hospital, Sweden the generated target was purified by dry distillation to achieve pure ^{211}At , as previously reported [22].

2.3. Preparation of Citrate-Stabilized 1st Generation AuNPs (1)

HAuCl₄·3H₂O (14.2 mg, 36 μmol) was first dissolved in MQ water (10 mL) and added to additional MQ water (90 mL) in a three-neck flask fitted with a reflux condenser. At the same time, a second solution was prepared in a metal-free plastic tube by dissolving fresh trisodium citrate (84 mg, 328 μmol) in MQ water (8 mL). The gold solution was then heated to 80 °C and the trisodium citrate solution was added in one portion under vigorous mixing. The reaction mixture was stirred for 60 min at 80 °C, until the color changed to a dark red.

2.4. Preparation of Citrate-Stabilized 2nd Generation AuNPs (3)

In a three-neck flask fitted with a reflux condenser, 20 mL of the 1st generation Au-nanoparticles was diluted with MQ water (80 mL). Fresh trisodium citrate solution was prepared by dissolving trisodium citrate dihydrate (21.2 mg, 82 μmol) in MQ water (2.0 mL). After mixing the two solutions and heating to 80 °C, a solution of HAuCl₄ (18.5 mg, 47 μmol, 3 mM) in MQ water (15 mL) was added dropwise over 30 min to provide 2nd generation AuNPs.

2.5. Surface Adsorption of ²¹¹At to 2nd Generation AuNPs (5, 7, Group A, Group B)

In a 10 mL flask, 5 mL of the 2nd generation AuNP dispersion was placed. To this solution, 29.5 MBq of ²¹¹At in CHCl₃ (20 μL) was added. The mixture was stirred for 20 min at room temperature and was subsequently heated to 80 °C for 60 min.

2.6. Embedding of ²¹¹At in 2nd Generation AuNPs (6, Group C)

In a 10 mL flask, 1 mL of the 1st generation AuNPs was dissolved in MQ water (4 mL). To this mixture, 29.5 MBq of ²¹¹At in CHCl₃ (20 μL) was added. After 20 min stirring at room temperature, trisodium citrate (1.06 mg, 3.6 μmol) in MQ water (100 μL) was added. After this mixture reached a temperature of 80 °C, HAuCl₄·3H₂O (0.93 mg, 2.25 μmol) in MQ water (750 μL) was added in three portions of 250 μL over 6 min. This mixture was stirred at 80 °C for an additional 60 min.

2.7. PEG Coating of 2nd Generation AuNPs (4, 7, 8)

For 4.6 mL of 2nd generation AuNPs (c_{Au} = 0.441 mM), HS-PEG₅₀₀₀ (0.74 mg) was weighted out and dissolved in MQ water (484 μL). This solution was then added to the AuNPs and stirred for 25 min at room temperature. The AuNPs were purified by transferring them to Amicon[®] centrifugal filter devices (30 kDa) and concentrating them by centrifugation to ca. 100 μL for 5 min at 4.4 krpm. The obtained residue was resuspended in HEPES buffer. The centrifugation and resuspension was repeated 5 times.

2.8. Oxidative Stability Test

In a centrifuge filter, 0.5 mL of the ²¹¹At-AuNP dispersion was mixed with aq. sodium hypochlorite (0.25 mL, 6–14% active Cl₂). This mixture was shaken for 5 min at room temperature. The color of the solution changed from dark red to colorless and a black precipitate was formed. To this precipitate, water (2.0 mL) was added and the mixture was centrifuged for 5 min at 4.4 krpm. The addition of water and centrifugation was repeated 3 times and the washing water phases combined. The activity from the combined water phases and the activity in the filter were measured on a well counter.

2.9. Serum Stability Test

A mixture of 100 μL of the PEG-coated [²¹¹At]AuNPs in HEPES buffer was diluted with HEPES buffer (600 μL) and mouse serum (300 μL) and was shaken for 4 h at 37 °C at room temperature. After 4 h, MeOH (1 mL) was added and the mixture was shaken for an additional 5 min. In the next step, DCM (2 mL) was added and the resulting suspension was shaken for an additional 5 min. The mixture was centrifuged for 10 min at 4.4 krpm, resulting in a phase separation between the organic and the aqueous phases, separated by a

“cake” of agglomerated proteins and serum components. The fractions were separated and each fraction was individually washed twice by adding 2 mL of water to the organic phase, 2.0 mL of DCM to the aqueous phase and 2 mL water to the “protein-cake”. The combined organic phase, the combined aqueous phase, and the protein cake were measured on a well counter.

2.10. ICP Determination of Gold Content for the Serum Stability Test

Each phase obtained from the procedure described above was dried at 50 °C, overnight. To each fraction was then added aq. HNO₃ (500 µL, 16 M), aq. H₂O₂ (300 µL, 10 M), and aq. HCl (50 µL, 11 M). The solutions were stirred for 20 h at 65 °C. The mixtures were then diluted with aq. HCl (14.2 mL, 3.7 M). A standard curve for gold was prepared, and each sample was measured by ICP-OES.

2.11. In Vivo Stability Study

The PEG-coated 2nd gen ²¹¹At-AuNPs were concentrated using an Amicon[®] centrifugal filter device (4 min, 4.4 krpm) and then washed 3 times with HEPES buffer. Finally, they were resuspended in HEPES buffer to achieve a final radioactivity concentration of 8–9 MBq/mL. For the free ²¹¹At control, HEPES buffer was added to dry ²¹¹At, dissolving it to the same concentration. The biodistribution of all samples was evaluated in healthy female Balb/C nu/nu mice (Janvier Labs, France), 4–6 weeks of age. This study was approved by the Gothenburg Ethical Committee for Animal Research (Ethical permit: 283-2011), and all animals were maintained as regulated by the Swedish Animal Welfare Agency. The mice were housed under sterile conditions at 22 °C with access to food and water ad libitum. Approximately 0.8–0.9 MBq of ²¹¹At in 100 µL was intravenously injected through the tail vein in a total of 18 mice. The mice were sacrificed at 21 h after injection. Blood was collected by cardiac puncture and tissues including thyroid/throat, salivary glands, heart, lungs, liver, stomach, kidneys, and spleen were excised. The tissues were weighed and ²¹¹At activity was measured on a NaI(Tl) γ-counter (Wizard 1480, Wallac, Finland). Results were expressed as the percent of injected dose per gram of organ (% ID/g).

3. Results and Discussion

3.1. Gold Nanoparticle Preparation

AuNPs with surface adsorbed ²¹¹At were prepared by three different methods (Figure 2). This resulted in Group A: Direct ²¹¹At adsorption onto PEG-precoated AuNPs, Group B: Direct ²¹¹At adsorption onto citrate-stabilized AuNPs, followed by PEG-coating, and Group C: An embedding procedure for doping AuNPs with ²¹¹At, inspired by our previous work [23].

A modified version of the Turkevich–Frens method [24,25] was employed for AuNP synthesis. Hydrogen-tetrachloroaurate(III) trihydrate (HAuCl₄·3H₂O) was reduced by adding aqueous sodium citrate at 80 °C, forming the first generation (1st gen, 1–2) AuNPs (16.3 ± 1.3 nm). Besides reducing the gold, citrate also stabilizes the formed AuNPs in aqueous dispersion by electrostatic interaction with the AuNP surface. Second generation (2nd gen, 3–8) AuNPs were formed by heating 1st gen AuNPs (1) to 80 °C with addition of aqueous HAuCl₄ over 10 min (28.5 ± 3.3 nm). To improve the biocompatibility of the AuNPs, the surface-bound citrate was displaced by a neutrally-charged HS-polyethyleneglycol-5000 (HS-PEG₅₀₀₀) coating to yield 4, 7, and 8. Such a coating is known to provide plasma circulation half-lives in mice of approximately 10–20 h [23,26]. PEG forms a hydrated corona around the AuNPs, which sterically impedes interaction with other blood components [27,28]. Successful coating with HS-PEG₅₀₀₀ was confirmed by an increase in the hydrodynamic diameter from 28.5 ± 3.3 nm to 51.6 ± 3.9 nm, as measured by dynamic light scattering (DLS) (Figure 3A), and a decrease in surface charge from −19.9 ± 2.1 mV to −11.6 ± 1.4 mV (Figure 3C).

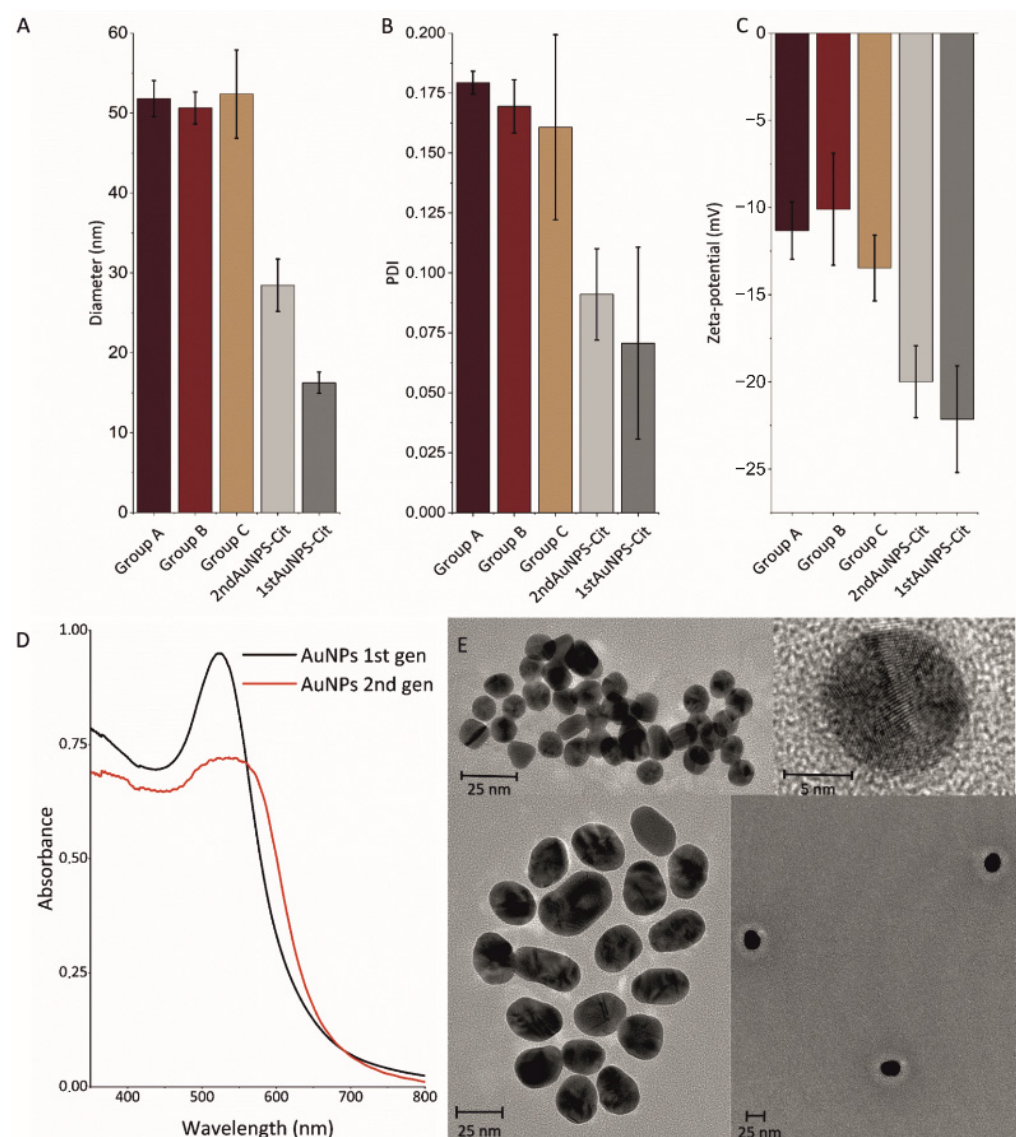


Figure 3. Characterization of AuNPs. Groups A, B and C are shown, along with 2nd gen citrate-stabilized AuNPs, measured by DLS ($n = 3$). (B) Polydispersity indices (PDIs) derived from the DLS measurements ($n = 3$). (C) Zeta potentials measured by DLS ($n = 2$). (D) UV-VIS absorption spectra of 1st and 2nd generation citrate-stabilized AuNPs. (E) Transmission electron microscopy (TEM) pictures of 1st generation citrate-stabilized AuNPs (top) and second generation HS-PEG₅₀₀₀-coated AuNPs (bottom). In the bottom-right image, a pale corona around the AuNPs indicates successful PEG coating. By analyzing the TEM-images, an average size of $11.9 \text{ nm} \pm 0.8 \text{ nm}$ ($n = 113$) for the first generation citrate-stabilized AuNPs (1) was found and for the second generation HS-PEG₅₀₀₀-coated AuNPs (4), an average size of $25.3 \text{ nm} \pm 2.1 \text{ nm}$ ($n = 201$) was found.

3.2. Radiolabeling with ^{211}At

Three different 2nd gen HS-PEG₅₀₀₀-coated ^{211}At -AuNPs were prepared by different routes, resulting in Groups A, B and C. The synthesis of all groups started from 1st gen citrate-stabilized AuNPs (1). In Group A and Group B, a second layer of gold was added directly onto the 1st gen AuNPs, which led to an increase in size, as observed by DLS and transmission electron microscopy (TEM) (Figure 3A,E). Groups A and B differed in the stage at which ^{211}At was added. In Group A, ^{211}At was added after PEG-coating, while in Group B, ^{211}At was added first, after which the AuNPs were coated with PEG. This differentiation was chosen to investigate whether stable surface labeling with ^{211}At could

be achieved both before and after PEG coating. In Group C, an embedding procedure was attempted [22,29]. In this group, ^{211}At was added to the 1st gen citrate-stabilized AuNPs to give, followed by the addition of a 2nd layer of gold, as described above. This was to investigate whether ^{211}At can be stably trapped inside AuNPs, as we have previously shown for copper-64 [22]. After the radiolabeling procedures were carried out, the resulting ^{211}At -AuNPs were purified and washed on centrifuge filters with pore sizes of 30 kDa. The combined aqueous filtrates were collected and the ^{211}At content in these and in the purified ^{211}At -AuNPs were quantified. In all three groups, >99% of the radioactivity remained with the AuNPs, demonstrating highly efficient radiolabeling and a quantitative radiochemical yield (RCY).

3.3. Stability Evaluation by Oxidative Challenge

The stability of the ^{211}At radiolabel for each group was first evaluated chemically. Sodium hypochlorite, a strong oxidant, was added to the ^{211}At -AuNPs. This treatment was intended to break the Au-At association on the surface of the ^{211}At -AuNPs, by oxidizing the ^{211}At . Upon addition of the oxidant, AuNP agglomeration was immediately observed as the appearance changed from a dark red dispersion to black precipitate suspended in a transparent, colorless liquid. This was likely caused by oxidation of the thiols binding the coating to the AuNPs, resulting in non-stabilized AuNPs. The AuNP precipitate was isolated on a centrifuge filter and the activity in both fractions was measured in a dose calibrator. ^{211}At not associated with the AuNPs would pass through and appear in the filtrate. This was confirmed by a control experiment in which AuNPs were excluded, where all activity (3.8 MBq of ^{211}At) passed through the filter. For Group C, the embedding group, $51.2 \pm 5.2\%$ of the activity was associated with the AuNP precipitate. A similar result was observed for Group A ($48.9 \pm 7.6\%$) and Group B ($47.8 \pm 8.2\%$), with no significant difference between the three groups. This led to the conclusion that all three methods resulted in ^{211}At -radiolabels of similar stability. Accordingly, the embedding (Group C) did not appear to have resulted in ^{211}At stably trapped inside the AuNPs in a yield that would provide a superior stability towards challenge by oxidation, as compared to surface adsorption.

3.4. Stability Evaluation in Serum

The radiolabel stability of the three groups was further evaluated by incubation in mouse serum over 4 h at 37°C , with free ^{211}At also incubated as control (Figure 4). To better complement the results obtained by Bilewicz and co-workers [19], a new method was developed for evaluating potential ^{211}At loss from the AuNPs. After incubation in serum, methanol (MeOH) and dichloromethane (DCM) were added to precipitate the serum components. Upon centrifugation of the resulting heterogeneous mixtures, a clear segregation of biological material into a middle layer was achieved (Figure 4B). This created a three-phase system consisting of polar medium ("aqueous"), apolar medium ("DCM") and serum component precipitate ("protein cake"). Both the bottom DCM phase and the protein cake were red-colored, indicating the presence of AuNPs in these two phases, whereas the aqueous phase was colorless. This was confirmed in a control experiment where the gold content in all three fractions was measured by inductively-coupled plasma atomic emission spectroscopy (ICP-OES) (Figure 4A); $56.3 \pm 3.5\%$ of the gold was found in the "protein-cake", $41.4 \pm 1.9\%$ in the organic phase and $2.3 \pm 2.6\%$ in the aqueous phase. We consider it likely that the presence of AuNPs in the protein cake was due to co-precipitation with serum components. The ^{211}At -AuNPs were primarily found in the bottom DCM phase [30]. In contrast, free ^{211}At was located almost exclusively in the top aqueous phase, as was confirmed in a control experiment in which free ^{211}At was incubated with mouse serum. Here, $98.8 \pm 1.1\%$ of the activity was found in the aqueous phase (Figure 4A). This also showed that when free ^{211}At is added to serum, it does not associate with proteins, as negligible activity was found in the protein-cake. For the ^{211}At -AuNP Groups A–C, the opposite was observed. Over 95% of the ^{211}At was found in the

combined AuNP-containing phases (“protein cake” and “DCM”). As free ^{211}At in the control experiment did not associate with these two phases to any significant extent, it was concluded that >95% of the added activity remained on the ^{211}At -AuNPs in all three groups and that the ^{211}At -radiolabel was highly stable in serum.

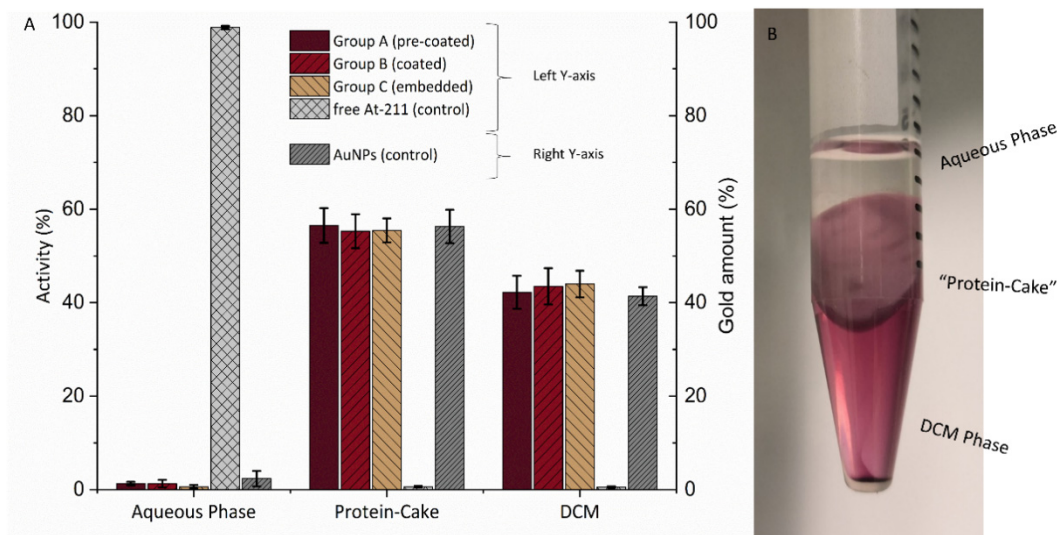


Figure 4. Serum stability of the ^{211}At -AuNPs in mouse serum. (A) Stability of the ^{211}At -AuNPs in mouse serum after 4 h at 37 °C (n = 3) compared to a control group of free ^{211}At (left axis). The gold content in each fraction was analyzed by ICP-OES (right axis) and was observed to correlate with activity for the AuNP samples, indicating high stability of the ^{211}At -radiolabel in all groups. (B) This image shows the distribution of PEG-coated ^{211}At -AuNPs observed as red coloration between the aqueous phase (top), the “protein-cake” (middle) and the DCM phase (bottom), after centrifugation.

3.5. In Vivo Stability Evaluation in Mice

The in vivo stability of the ^{211}At -radiolabel was investigated for Group B–C. This was carried out in healthy Balb/c mice, through quantification of the biodistribution by ex vivo well-counting of key organs and tissues (Figure 5). Groups B and C were chosen since the preceding experiments described above had shown no difference between Groups A and B, and we desired to investigate whether embedding (Group C) provided an advantage in vivo that had not been detected in our in vitro evaluation. An activity of 0.8–0.9 MBq was administered intravenously in all cases; 21 h post-injection, the mice were sacrificed, and organs were resected, weighed, and the ^{211}At -activities measured. ^{211}At -AuNP Groups B and C were compared statistically to the control group of free ^{211}At in HEPES-buffer, via a one-way ANOVA with post hoc Tukey’s test (Figure 5).

A pronounced and generally statistically significant difference between the free ^{211}At and the two ^{211}At -AuNP groups was observed. The biodistribution of free ^{211}At was comparable to previously reported data [31], with pronounced accumulation occurring primarily in the thyroid ($10.0 \pm 1.7\%$ ID/g) and stomach ($9.3 \pm 1.9\%$ ID/g). Around 3% ID/g was detected in lungs, salivary glands and spleen. The remaining activity is likely to have been excreted or located to un-analyzed tissues. In contrast, Groups B and C showed limited accumulation in the thyroid, which in both cases was highly significantly different from free ^{211}At , at $3.7 \pm 0.5\%$ ID/g ($p = 0.011$) and $4.2 \pm 1.1\%$ ID/g ($p = 0.015$), respectively. A similar difference was observed for stomach, with Groups B and C showing $3.2 \pm 0.7\%$ ID/g ($p = 0.024$) and $4.5 \pm 1.3\%$ ID/g ($p = 0.075$), respectively. Accordingly, the two ^{211}At -AuNP groups exhibited low uptake in the two hallmark accumulation tissues of free ^{211}At , testifying to a high stability of the ^{211}At -radiolabel.

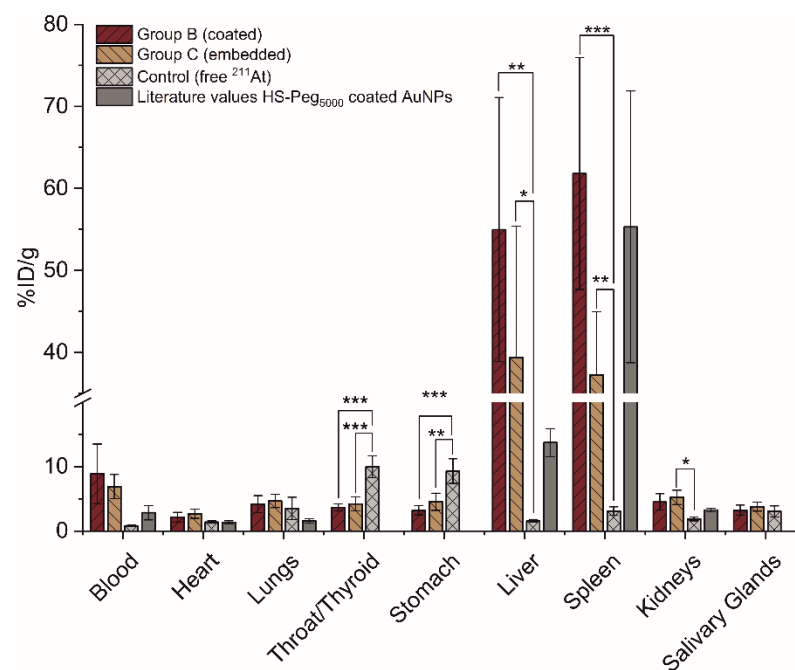


Figure 5. Ex vivo biodistribution analysis at 21 h post-injection of ²¹¹At-AuNPs as Groups B and C (n = 5) and free ²¹¹At (n = 3), administered to healthy Balb/c mice. In the figure, literature values of the biodistribution of AuNPs with a similar size (73 ± 6 nm) and the same coating materials (HS-PEG₅₀₀₀) were included [23]. The data were analyzed by a one-way ANOVA followed by a Tukey's multiple comparison test with the following significance thresholds (*) $p > 0.3$, (**) $p > 0.15$, (***) $p < 0.025$.

It should be noted that the small but detectable presence of ²¹¹At-AuNPs observed in thyroid and stomach for Groups B and C could be due to perfusion of these organs by ²¹¹At-AuNP-containing blood. A substantial difference was observed in the blood concentration at 21 h between the two ²¹¹AuNP groups and free ²¹¹At, with $8.9 \pm 4.6\%$ ID/g (Group B) and $6.9 \pm 1.9\%$ ID/g (Group C), compared to a very low $0.8 \pm 0.1\%$ ID/g for the free ²¹¹At. Accordingly, AuNP-bound ²¹¹At was significantly longer circulating than free ²¹¹At, suggesting that ²¹¹At bound to AuNPs in this way is stable in circulation. Due to variation in the data, blood content differences were not statistically different, however. PEG-coated AuNPs are expected to circulate long enough for an appreciable amount to be present in blood after 21 h. For reference, data from a previous study [23] has been included in Figure 5, showing typically observed ex vivo biodistribution data for this size range of AuNPs, in this case, obtained 24 h post-injection, with blood circulation still present at this time (2.8% ID/g).

In Groups B and C, the majority of the ²¹¹At was found in the liver and the spleen, which is consistent with generally observed nanoparticle biodistribution, as observed from the reference data included in Figure 5 and general literature [23,32]. In Groups B and C, $55.0 \pm 16.1\%$ ID/g and $39.4 \pm 16.0\%$ ID/g accumulated in the liver, compared to very low uptake of free ²¹¹At at $1.6 \pm 0.2\%$ ID/g. Similarly, $61.8 \pm 14.1\%$ ID/g and $37.3 \pm 7.7\%$ ID/g accumulated in the spleen, respectively, with similarly low uptake of free ²¹¹At at $3.1 \pm 0.6\%$ ID/g. This data also supports the conclusion that surface adsorbed ²¹¹At on AuNPs follows the general biodistribution of nanoparticles, and is therefore of high stability in circulation. In addition, liver and spleen uptake of nanoparticles is mediated by macrophage phagocytosis [33] and ²¹¹At is considered non-residualizing [9,34]. This means that if ²¹¹At detached from the nanoparticles during macrophage phagocytosis, it would exhibit free ²¹¹At behavior upon excretion from macrophages and therefore lead to thyroid and stomach accumulation. Since liver and spleen uptake is preserved at 21 h, this further attests to the excellent stability of the surface-adsorbed ²¹¹At.

Between the two ^{211}At -AuNP groups themselves (Group B and Group C), no substantial differences were observed. This supports our preceding stability evaluations, serum and oxidative challenge, in that no difference between embedding of ^{211}At (Group C) versus surface adsorption (Groups A and B) exists. Both ^{211}At -AuNP types showed high in vivo stability, irrespective of whether an embedding procedure had been carried out or not. Further, since the evaluation by oxidative challenge showed only $52 \pm 5.2\%$ associated with the AuNPs, we conclude that the embedding procedure was not successful and hypothesize that surface-adsorbed ^{211}At continues to move with and stay on the surface as more gold is added onto the AuNPs. In turn, however, embedding does not appear to be a prerequisite to obtain high in vivo stability, as this is also observed with surface adsorption.

Accordingly, our results demonstrate a high general stability of ^{211}At that is surface-adsorbed to AuNP surfaces. AuNPs are a versatile drug delivery platform with significant potential. The advantages of AuNPs primarily rest in their biocompatibility, their facile surface functionalization with thiol-bearing derivatives, and the fact that they can be prepared in a wide range of sizes (ca. 2–70 nm) and shapes [35–37]. Functionalization with targeting vectors further allows for the specific receptor targeting to desired cells and surface structures, with cancer cells being of particular relevance [38,39]. The results we present here demonstrate the potential in using ^{211}At with AuNP-based drug delivery systems for targeted alpha therapy (TAT). A particular advantage with TAT is that no drug release is required. Instead, surface adsorbed ^{211}At will emit alpha particles that can strike and kill targeted cancer cells from a distance. It should be noted that the range in gold of alpha particles emitted from ^{211}At is about 10 μm (own calculations). This means that the alpha particles will not be absorbed by the AuNPs themselves, even if they traverse it along the full length of their diameter.

4. Conclusions

In this study, we report high in vitro and in vivo stability of ^{211}At attached to AuNPs by surface adsorption. This was achieved by adding ^{211}At to preformed AuNPs, giving excellent radiochemical yields of >99%. The resulting ^{211}At -radiolabel was partly stable ($48.3 \pm 3.2\%$) under very harsh oxidative conditions, while completely stable in serum for up to four hours (>95%). Finally, we demonstrated high in vivo stability of the surface-adsorbed ^{211}At in healthy mice for up to 21 h. Due to the facile and non-specific radiolabeling method, the surface of the ^{211}At -labeled AuNPs is likely to be modifiable with tumor-targeting vectors. This method for labeling AuNPs with ^{211}At therefore appears to be relevant and useful as a delivery system for ^{211}At in targeted radionuclide therapy.

Author Contributions: Conceptualization, A.K., M.M.H. and A.I.J.; methodology, E.S., S.L., E.A., H.J., T.B., P.J.K. and A.I.J.; formal analysis, E.S. and A.I.J.; investigation, E.S., C.B.M.P., A.I.J., H.J., S.L., E.A., T.B. and P.J.K.; resources, S.L., T.B., A.K., M.M.H. and A.I.J.; writing—original draft preparation, E.S., C.B.M.P., M.M.H. and A.I.J.; writing—review and editing, all authors; visualization, E.S.; supervision, M.M.H. and A.I.J.; project administration, A.K., M.M.H. and A.I.J.; funding acquisition, A.K., M.M.H., A.I.J., S.L. and T.B. All authors have read and agreed to the published version of the manuscript.

Funding: This research was funded by the Independent Research Fund Denmark, grant number 8022-00358B.

Institutional Review Board Statement: This study was approved by the Gothenburg Ethical Committee for Animal Research (Ethical permit: 283-2011), and all animals were maintained as regulated by the Swedish Animal Welfare Agency. The mice were housed under sterile conditions at 22 °C with access to food and water ad libitum.

Acknowledgments: This work acknowledges the EU Cost Action CA19114—Network for Optimized Astatine labeled Radiopharmaceuticals (NOAR).

Conflicts of Interest: The authors declare no conflict of interest.

References

1. Jadvar, H. Targeted α -Therapy in Cancer Management: Synopsis of Preclinical and Clinical Studies. *Cancer Biother. Radiopharm.* **2020**, *35*, 475–484. [CrossRef]
2. Denk, C.; Wilkovitsch, M.; Aneheim, E.; Herth, M.M.; Jensen, H.; Lindegren, S.; Mikula, H. Multifunctional Clickable Reagents for Rapid Bioorthogonal Astatination and Radio-Crosslinking. *ChemPlusChem* **2019**, *84*, 775–778. [CrossRef] [PubMed]
3. Dizdarevic, S.; Jessop, M.; Begley, P.; Main, S.; Robinson, A. (223)Ra-Dichloride in castration-resistant metastatic prostate cancer: Improving outcomes and identifying predictors of survival in clinical practice. *Eur. J. Nucl. Med. Mol. Imaging* **2018**, *45*, 2264–2273. [CrossRef] [PubMed]
4. Kratochwil, C.; Bruchertseifer, F.; Rathke, H.; Hohenfellner, M.; Giesel, F.L.; Haberkorn, U.; Morgenstern, A. Targeted α -Therapy of Metastatic Castration-Resistant Prostate Cancer with 225Ac-PSMA-617: Swimmer-Plot Analysis Suggests Efficacy Regarding Duration of Tumor Control. *J. Nucl. Med.* **2018**, *59*, 795–802. [CrossRef] [PubMed]
5. Sathekge, M.; Bruchertseifer, F.; Knoesen, O.; Reyneke, F.; Lawal, I.; Lengana, T.; Davis, C.; Mahapane, J.; Corbett, C.; Vorster, M.; et al. 225Ac-PSMA-617 in chemotherapy-naive patients with advanced prostate cancer: A pilot study. *Eur. J. Nucl. Med. Mol. Imaging* **2019**, *46*, 129–138. [CrossRef] [PubMed]
6. Parker, C.; Lewington, V.; Shore, N.; Kratochwil, C.; Levy, M.; Lindén, O.; Noordzij, W.; Park, J.; Saad, F. Targeted Alpha Therapy, an Emerging Class of Cancer Agents: A Review. *JAMA Oncol.* **2018**, *4*, 1765–1772. [PubMed]
7. Makvandi, M.; Dupis, E.; Engle, J.W.; Nortier, F.M.; Fassbender, M.E.; Simon, S.; Birnbaum, E.R.; Atcher, R.W.; John, K.D.; Rixe, O.; et al. Alpha-Emitters and Targeted Alpha Therapy in Oncology: From Basic Science to Clinical Investigations. *Target. Oncol.* **2018**, *13*, 189–203. [CrossRef]
8. Pantel, K.; Cote, R.J.; Fodstad, Ø. Detection and Clinical Importance of Micrometastatic Disease. *JNCI J. Natl. Cancer Inst.* **1999**, *91*, 1113–1124. [CrossRef]
9. Lindegren, S.; Albertsson, P.; Bäck, T.; Jensen, H.; Palm, S.; Aneheim, E. Realizing Clinical Trials with Astatine-211: The Chemistry Infrastructure. *Cancer Biother. Radiopharm.* **2020**, *35*, 425–436. [CrossRef]
10. Berei, K.; Vasaros, L. Organic Chemistry of Astatine, Hungarian Academy of Sciences Report, 1981, KFKI-1981-10. Available online: https://inis.iaea.org/collection/NCLCollectionStore/_Public/12/609/12609573.pdf?r=1 (accessed on 29 September 2021).
11. Milius, R.A.; McLaughlin, W.H.; Lambrecht, A.P.; Carroll, J.J.; Adelstein, S.J. Organoastatine chemistry. Astatination via electrophilic destannylation. *Appl. Radiat. Isot.* **1986**, *37*, 799–802. [CrossRef]
12. Zalutsky, M.R.; Garg, P.K.; Friedman, H.S.; Bigner, D.D. Labeling of monoclonal antibodies and F(ab')₂ fragments with the α -particle-emitting nuclide At-211: Preservation of immunoreactivity and in vivo localizing capacity. *Proc. Natl. Acad. Sci. USA* **1989**, *86*, 7149–7715. [CrossRef] [PubMed]
13. Andersson, H.; Elgqvist, J.; Horvath, G.; Hultborn, R.; Jacobsson, L.; Jensen, H.; Karlsson, B.; Lindegren, S.; Palm, S. Astatine-211-labeled antibodies for treatment of disseminated ovarian cancer: An overview of results in an ovarian tumor model. *Clin. Cancer Res.* **2003**, *9*, 3914S–3921S. [PubMed]
14. Hadley, W.S.; Wilbur, D.S.; Gray, M.A.; Atcher, W.R. Astatine-211 labeling of an antimelanoma antibody and its Fab fragment using N-succinimidyl p-[211At] astatobenzoate: Comparisons in vivo with the p-[125I] iodobenzoyl conjugate. *Bioconjug. Chem.* **1991**, *2*, 171–179. [CrossRef] [PubMed]
15. Teze, D.; Sergentu, D.C.; Kalichuk, V.; Barbet, J.; Deniaud, D.; Galland, N.; Maurice, R. Targeted radionuclide therapy with astatine-211: Oxidative dehalogenation of astatobenzoate conjugates. *Sci. Rep.* **2017**, *7*, 2579. [CrossRef]
16. Kucka, J.; Hruby, M.; Konak, C.; Kozempel, J.; Lebeda, O. Astatination of nanoparticles containing silver as possible carriers of 211At. *Appl. Radiat. Isot.* **2006**, *64*, 201–206. [CrossRef]
17. Cedrowska, E.; Łyczko, M.; Piotrowska, A.; Bilewicz, A.; Stolarz, A.; Trzcińska, A.; Szkliar, K.; Waś, B. Silver impregnated nanoparticles of titanium dioxide as carriers for 211At. *Radiochim. Acta* **2016**, *104*, 267–275. [CrossRef]
18. Jeong, E.H.; Jung, G.; Hong, C.A.; Lee, H. Gold nanoparticle (AuNP)-based drug delivery and molecular imaging for biomedical applications. *Arch. Pharm. Res.* **2014**, *37*, 53–59. [CrossRef] [PubMed]
19. Dziawer, L.; Kozminski, P.; Meczynska-Wielgosz, S.; Pruszyński, M.; Łyczko, M.; Waś, B.; Celichowski, G.; Grobelny, J.; Jastrzebski, J.; Bilewicz, A. Gold nanoparticle bioconjugates labelled with 211At for targeted alpha therapy. *RSC Adv.* **2017**, *7*, 41024–41032. [CrossRef]
20. Dziawer, L.; Majkowska-Pilip, A.; Gawęł, D.; Godlewska, M.; Pruszyński, M.; Jastrzebski, J.; Waś, B.; Bilewicz, A. Trastuzumab-Modified Gold Nanoparticles Labeled with 211At as a Prospective Tool for Local Treatment of HER2-Positive Breast Cancer. *Nanomaterials* **2019**, *9*, 632. [CrossRef]
21. Ostrowski, S.; Majkowska-Pilip, A.; Bilewicz, A.; Dobrowolski, J.C. On Au_nAt clusters as potential astatine carriers. *RSC Adv.* **2017**, *7*, 35854–35857. [CrossRef]
22. Lindegren, S.; Bäck, T.; Jensen, H.J. Dry-distillation of astatine-211 from irradiated bismuth targets: A time-saving procedure with high recovery yields. *Appl. Radiat. Isot.* **2001**, *55*, 157–160. [CrossRef]
23. Frellsen, A.F.; Hansen, A.E.; Jøck, R.I.; Kempen, P.J.; Severin, G.W.; Rasmussen, P.H.; Kjær, A.; Jensen, A.T.; Andresen, T.L. Mouse Positron Emission Tomography Study of the Biodistribution of Gold Nanoparticles with Different Surface Coatings Using Embedded Copper-64. *ACS Nano* **2016**, *10*, 9887–9898. [CrossRef]
24. Turkevich, J.; Stevenson, P.C.; Hillier, J. A Study of the Nucleation and Growth Processes in the Synthesis of Colloidal Gold. *Discuss. Faraday Soc.* **1951**, *11*, 55–75. [CrossRef]

25. Frens, G. Controlled Nucleation for the Regulation of the Particle Size in Monodisperse Gold Suspensions. *Nat. Phys. Sci.* **1973**, *241*, 20–22. [[CrossRef](#)]
26. Suk, J.S.; Xu, Q.; Kim, N.; Hanes, J.; Ensign, L.M. PEGylation as a strategy for improving nanoparticle-based drug and gene delivery. *Adv. Drug Deliv. Rev.* **2016**, *99*, 28–51. [[CrossRef](#)] [[PubMed](#)]
27. Zhang, G.; Yang, Z.; Lu, W.; Zhang, R.; Huang, Q.; Tian, M.; Li, L.; Liang, D.; Li, C. Influence of anchoring ligands and particle size on the colloidal stability and in vivo biodistribution of polyethylene glycol-coated gold nanoparticles in tumor-xenografted mice. *Biomaterials* **2009**, *30*, 1928–1936. [[CrossRef](#)] [[PubMed](#)]
28. Kristensen, K.; Engel, T.B.; Stensballe, A.; Simonsen, J.B.; Andresen, L.T. The hard protein corona of stealth liposomes is sparse. *J. Control. Release* **2019**, *307*, 1–15. [[CrossRef](#)]
29. Fach, M.; Fliedner, F.P.; Kempen, P.J.; Melander, F.; Hansen, A.E.; Bruun, L.M.; Köster, U.; Sporer, E.; Kjær, A.; Andresen, T.L.; et al. Effective Intratumoral Retention of [103Pd] AuPd Alloy Nanoparticles Embedded in Gel-Forming Liquids Paves the Way for New Nanobrachytherapy. *Adv. Healthc. Mater.* **2021**, *10*, 2002009. [[CrossRef](#)] [[PubMed](#)]
30. Alkilany, A.M.; Bani Yaseen, A.I.; Park, J.; Eller, J.R.; Murphy, C.J. Facile phase transfer of gold nanoparticles from aqueous solution to organic solvents with thiolated poly(ethylene glycol). *RSC Adv.* **2014**, *4*, 52676–52679. [[CrossRef](#)]
31. Spetz, J.; Rudqvist, N.; Forssell-Aronsson, E. Biodistribution and dosimetry of free 211At, 125I- and 131I- in rats. *Cancer Biother. Radiopharm.* **2013**, *28*, 657–664. [[CrossRef](#)]
32. Lipka, J.; Semmler-Behnke, M.; Sperling, R.A.; Wenk, A.; Takenaka, S.; Schleh, C.; Kissel, T.; Parak, W.J.; Kreyling, W.G. Biodistribution of PEG-modified gold nanoparticles following intratracheal instillation and intravenous injection. *Biomaterials* **2010**, *31*, 6574–6581. [[CrossRef](#)]
33. Gustafson, H.H.; Holt-Casper, D.; Grainger, D.W.; Ghandehari, H. Nanoparticle Uptake: The Phagocyte Problem. *Nano Today* **2015**, *10*, 487–510. [[CrossRef](#)]
34. Steffen, A.C.; Almqvist, Y.; Chyan, M.K.; Lundqvist, H.; Tolmachev, V.; Wilbur, D.S.; Carlsson, J. Biodistribution of 211At labeled HER-2 binding affibody molecules in mice. *Oncol. Rep.* **2007**, *17*, 1141–1147. [[CrossRef](#)]
35. Li, W.; Cao, Z.; Liu, R.; Liu, L.; Li, H.; Li, X.; Chen, Y.; Lu, C.; Liu, Y. AuNPs as an important inorganic nanoparticle applied in drug carrier systems. *Artif. Cells Nanomed. Biotechnol.* **2019**, *47*, 4222–4233. [[CrossRef](#)] [[PubMed](#)]
36. Dreaden, E.C.; Austin, L.A.; Mackey, M.A.; El-Sayed, M.A. Size matters: Gold nanoparticles in targeted cancer drug delivery. *Ther. Deliv.* **2012**, *3*, 457–478. [[CrossRef](#)] [[PubMed](#)]
37. Sztandera, K.; Gorzkiewicz, M.; Klajnert-Maculewicz, B. Gold Nanoparticles in Cancer Treatment. *Mol. Pharm.* **2019**, *16*, 1–23. [[CrossRef](#)] [[PubMed](#)]
38. Paciotti, G.F.; Myer, L.; Weinreich, D.; Goia, D.; Pavel, N.; McLaughlin, R.E.; Tamarkin, L. Colloidal gold: A novel nanoparticle vector for tumor directed drug delivery. *Drug Deliv.* **2004**, *11*, 169–183. [[CrossRef](#)] [[PubMed](#)]
39. Huang, X.; Peng, X.; Wang, Y.; Wang, Y.; Shin, D.M.; El-Sayed, M.A.; Nie, S. A reexamination of active and passive tumor targeting by using rod-shaped gold nanocrystals and covalently conjugated peptide ligands. *ACS Nano* **2010**, *4*, 5887–5896. [[CrossRef](#)] [[PubMed](#)]